HHS Public Access

Author manuscript

Nat Genet. Author manuscript; available in PMC 2017 September 29.

Published in final edited form as:

Nat Genet. 2017 March ; 49(3): 465–469. doi:10.1038/ng.3780.

Divergent effects of activating mutations on developmental Ras signaling

Yogesh Goyal[1,2,4], **Granton A. Jindal**[1,2,3,4], **José L. Pelliccia**[3], **Kei Yamaya**[2,3], **Eyan Yeung**[2,3], **Alan S. Futran**[1,2], **Rebecca D. Burdine**[3], **Trudi Schüpbach**[3], and **Stanislav Y. Shvartsman**[1,2,3,*]

[1]Department of Chemical and Biological Engineering, Princeton University, Princeton, NJ 08544

[2]The Lewis-Sigler Institute for Integrative Genomics, Princeton University, Princeton, NJ 08544

[3]Department of Molecular Biology, Princeton University, Princeton, NJ 08544

Germline mutations in the Ras pathway components are associated with a large class of human developmental abnormalities, collectively known as RASopathies, and characterized by a range of structural and functional phenotypes, including cardiac defects and neurocognitive delays[1,2]. While it is generally believed that RASopathies are caused by altered levels of pathway activation, the nature of signaling changes in developing tissues remains largely unknown[3,4]. We used assays with spatiotemporal resolution in *Drosophila melanogaster* (fruit fly) and *Danio rerio* (zebrafish) to quantify signaling changes caused by mutations in MEK, a core component of the Ras pathway, which is mutated in both RASopathies and cancers[5,6]. Surprisingly, we discovered that intrinsically active variants of MEK can both increase and reduce the levels of pathway activation *in vivo*. The sign of the effect depends on cellular context and implies that some of the emerging phenotypes in RASopathies may be caused by increased, as well as attenuated, levels of Ras signaling.

MEK is a ubiquitously expressed kinase that remains inactive until it is phosphorylated in response to extracellular signals, such as locally secreted ligands of receptor tyrosine kinases (RTKs)[7]. Reflecting the patterns of RTK activation, the activity of MEK is regulated in both space and time, providing tight control of the activation of its direct substrate, the extracellular signal-regulated kinase (ERK). Studies with cultured cells suggest that MEK variants identified in individuals with RASopathies and cancers are active even without upstream signals[5,6]. To examine this possibility more directly, we reconstituted a biochemical system comprising purified ERK2, variants of MEK1, and ATP (Fig. 1a, b). We found that four out of five examined disease-related variants cause strong ERK2 phosphorylation (dpERK) (Fig. 1c, Supplementary Fig. 1 and Supplementary Tables 1,2). This result establishes the intrinsic activity of these mutations and suggests that some of

*Corresponding author (stas@princeton.edu).

[4]Contributed equally

Author Contributions: Y.G., G.A.J., R.D.B, T.S., and S.Y.S. conceived and designed the project. Y.G., E.Y., A.S.F., and G.A.J. performed *in vitro* experiments; Y.G., and K.Y. performed experiments in *Drosophila*; Y.G. and S.Y.S. developed the model with inputs from G.A.J., and G.A.J. and J.L.P. performed experiments in zebrafish. Y.G. and G.A.J. analyzed the results. Y.G., G.A.J. and S.Y.S. wrote the manuscript with input from R.D.B and T.S.

Competing Finanical Interests: The authors declare no competing financial interests.

their effects in embryos may derive from ectopic pathway activation. At the same time, these mutations may affect cellular responses to endogenous inductive signals, resulting in altered kinetics of ERK activation. Thus, biological effects of activating mutations are likely to reflect a combination of ectopic pathway activation and altered responses to endogenous cues.

The early *Drosophila* embryo provides a powerful system for exploring both of these scenarios. We focused on the first wave of ERK signaling in the early blastoderm, when the embryo has a particularly simple anatomy, with a uniform field of nuclei arranged under a common plasma membrane. At this stage, ERK activation is triggered by a locally produced ligand (Trunk) via a uniformly expressed RTK (Torso), resulting in a pattern of ERK activation that is localized at the embryonic poles and is negligible in the middle of embryo (Fig. 2a)[8,9]. The fly embryo can thus be used to simultaneously assess the effects of activating mutations on endogenous signaling (poles) and their ability to trigger ectopic pathway activation (middle of the embryo).

We used the Gal4-UAS system to uniformly express the intrinsically active MEK variants (Supplementary Fig. 2) in the early embryo from a maternal pool of RNA and quantified their effects on ERK phosphorylation. Consistent with their ability to phosphorylate ERK in the absence of upstream signals, these variants induced a significant increase of ERK phosphorylation in the central region of precisely timed embryos (Fig. 2b-i and Supplementary Figs. 3,4,5). Remarkably, ERK phosphorylation was strongly reduced at the embryonic poles, to ~50% of their wild type levels (Fig. 2b-i and Supplementary Fig. 4). Thus, intrinsically active MEK variants have opposing effects on developmental ERK activation: they induce ectopic pathway activation and, surprisingly, strongly attenuate response to endogenous signals.

Importantly, both of these effects had major consequences on the subsequent stages of tissue patterning and morphogenesis. In particular, ectopic ERK activation in the central region of the embryo resulted in dramatic alterations in the expression of the gap genes, such as *tailless (tll)* (Fig. 3a and Supplementary Figs. 6,7,8,9), which play a critical role in regulating the segmentation along the anteroposterior axis[10]. Consequently, the larval cuticle produced by the embryos expressing active MEK variants had a range of patterning defects, from fused segments to complete loss of segmented pattern (Fig. 3b). These defects in gene expression and morphogenesis are fully consistent with the previously reported effects of other gain-of-function (GOF) mutations in the Ras pathway[11–13]. Note that these strong defects are triggered by ectopic levels of ERK activation that are significantly lower than the maximal levels of endogenous pathway activation at the poles (Fig. 2c-e).

Given the strong reduction of ERK activation at the poles, we asked whether these changes phenocopy the defects observed in response to genetic perturbations that either abolish or strongly attenuate Ras signaling. Some of the canonical defects associated with loss of ERK activation in the early embryo correspond to the loss of the most anterior head structures[11,14] and a so-called pole-hole phenotype[14,15], in which some of the nuclei at the posterior pole are displaced from the plasma membrane. These defects can be induced by the loss of the Torso receptor[11,16], by the loss of Raf[17], which activates and phosphorylates MEK, or by

strong RNAi knockdown of MEK itself (Fig. 3c,d and Supplementary Fig. 10). Remarkably, both loss of head structures (Fig. 3c) and a pole-hole phenotype (Fig. 3d) were induced by the constitutively active MEK1 variants. Hence, morphological defects resulting from activating mutations can have very different origins in different locations. Some defects, including disruption of the segmented pattern, are caused by ectopic signaling, while others, such as the pole-hole phenotype, reflect attenuated response to patterning signals.

What is the basis of these divergent effects of activating mutations? ERK activation can induce the expression of inhibitors that can negatively regulate signal transduction at multiple points along the pathway, establishing negative feedback[18,19]. As a consequence, precocious pathway stimulation induced by intrinsically active mutations can desensitize the pathway to future rounds of signaling. To illustrate this point, consider a mathematical model (Fig. 4 and Supplementary Fig. 11a,b) in which the pathway is stimulated by a sum of two inputs: The first input is localized in space and time (u[x,t]), mimicking the effects of normal inductive signals. The second input is uniform in space and time (u_0), mimicking the effects of intrinsically active mutations. Signaling levels (S) decay with first-order kinetics and trigger the expression of an inhibitor (I) that attenuates the combined effect of the two inputs (Supplementary Table 3).

Motivated by the localized activation of the Torso pathway, the inductive input is modeled as a pulse in both space and time. In the absence of activating mutations, signaling levels are negligible in cells that do not receive the inductive signal, as revealed by spatiotemporal reconstruction of ERK activation (Fig. 5a and Supplementary Fig. 12). The situation is different when mutations are present, since the pathway is stimulated throughout the system even before the inductive signals arrive. In this case, inductive inputs act on the background with a nonzero level of inhibitor(s), induced by precocious pathway stimulation resulting from the activating mutations. As a result, response to endogenous cues is strongly attenuated (Fig. 5b). According to the model, the sign of the effect of activating mutations, as revealed by the ratio of signal for WT to that for mutant, changes across the system, from negative in cells that receive endogenous signals to positive in the rest of the tissue (Fig. 5c and Supplementary Fig. 11c,d). The effect is dynamic and reflects spatially uniform pathway activation that precedes arrival of inductive cues. This is fully consistent with the reconstruction of such a ratio from staged embryos (Fig. 5d).

In this model, the feedback inhibitor senses the constitutive activity, accumulates over time, and desensitizes the cells which receive the endogenous signals at later times. Therefore, the feedback model predicts that the same effect is not limited to mutations in MEK and can be induced by any other means of spatially uniform and precocious pathway activation. To test this prediction, we examined ERK activation in embryos with two types of genetic perturbations. First, we used embryos carrying a strong activating mutation in Torso (Tor^{D4021})[13]. Second, we used embryos with spatially uniform expression of PTTH, another ligand of Torso[20]. Consistent with the model, in both cases, we observed ectopic ERK activation in the middle of the embryo and strong reduction at the poles (Fig. 5e,f and Supplementary Fig. 13). To summarize, the divergent effects of activating mutations are not limited to MEK and can be induced by activating perturbations in other components of the RTK pathway. Indeed, a few studies have associated loss-of-function phenotypes with

activating mutations in the Ras pathway[21,22]. Our results suggest that such phenotypes may result from attenuated signaling levels. It is likely that multiple negative regulators work together to reduce ERK activity at the poles. In the future, these regulators can be identified following a combination of candidate gene and unbiased approaches.

We expect that the opposing effects of activating mutations revealed by our experiments in *Drosophila* represent a general property of developmental signaling by locally activated RTKs. As a first step towards testing this hypothesis, we focused on ERK activation in the zebrafish embryo during epiboly. During this stage, ERK signaling is triggered by locally produced Fibroblast Growth Factor (FGF) ligand, via uniformly expressed FGF receptor (FGFR), resulting in a pattern of ERK activation that is localized at the blastoderm margin and negligible in the animal cap[23]. We used mRNA injection to induce mosaic expression of MEK1 variants in the early embryo, facilitating quantitative spatial comparisons of ERK activation (Fig. 6a). In the animal cap, which does not receive endogenous Ras signaling in wild type embryos, MEK variants caused ectopic ERK activation (Fig. 6a-c and Supplementary Figs. 14a,15,16a,b). In the blastoderm margin, however, we observed attenuated ERK activation, consistent with our observations in *Drosophila* (Fig. 6a,d,e and Supplementary Figs. 14,15,16). Furthermore, while ectopic signaling results in an oval-embryo shape, a GOF defect, it is likely that reduced signaling at the blastoderm margin results in shorter cilia in Kupffer's vesicle, (Fig. 6f-i), a phenotype associated with loss of FGF signaling[24,25]. Thus, similar to observations in *Drosophila*, activating mutations in MEK1 cause ectopic signaling and attenuate response to endogenous inputs to RTKs.

To summarize, our results underscore the complexity of signaling changes that can be induced by the activating mutations in components of the Ras pathway. We found that the magnitude and even the sign of the effect may vary *in vivo*. Therefore, the structural and morphological defects observed in individuals with these mutations may have different origins: some defects may result from ectopic signaling while other defects may result from attenuated sensitivity to inductive cues. In the future, this possibility should be tested in the mammalian models of RASopathies and should be kept in mind when considering the proposed pharmacological treatments of RASopathies using the existing inhibitors of Ras signaling. In light of our data, predicting the results of these treatments is nontrivial. Since some of the phenotypes may be caused by a decrease or loss of ERK signaling, uniform inhibition of ERK signaling may correct only some of the defects and can potentially worsen others. Going beyond the RAS pathway, it will be important to test whether divergent effects on pathway activation can be caused by activating mutations in other signal transduction pathways[26–28].

Methods

Plasmid construction, protein expression, and protein purification for *in vitro* reactions

The pET28 plasmid containing N-terminally His_6 tagged MEK1 was a gift from Dr. Goldsmith (UTSW, Dallas). Plasmids containing N-terminally tagged mutant MEK1 gene sequences were constructed by overlap PCR of 5′- and 3′- ends of the genes produced by standard PCR using primers containing the desired mutation. The MEK1 mutant inserts and pET28 plasmid were digested using the same restriction enzymes used to clone wild type

MEK1 into pET28 (BamHI and XhoI), ligated, and transformed into *E. coli* for plasmid amplification and protein expression. The N-terminally His_6 tagged ERK2 expression construct was produced by standard PCR amplification of the ERK2 sequence, digestion of the gene and pQE80 plasmid by BamHI and HindIII, ligation, and transformation into *E. coli* for plasmid amplification and protein expression.

For the expression of MEK variants, pET28 plasmids encoding MEK variants were transformed into *E. coli* BL21(DE3) competent cells. Overnight cultures were sub-cultured into 1.5 L LB medium supplemented with 35 μg/mL kanamycin to a starting OD_{600} of 0.02. Cultures were grown at 37 °C with agitation at 250 RPM until they reached OD_{600} 0.9-1.1. Protein expression was induced by the addition of isopropyl-β-D-1-thiogalactopyranoside (IPTG) to a final concentration of 0.5 mM and cultures were grown for 6 hours at 25 °C with agitation at 200 RPM. Cells were harvested by centrifugation and cell pellets were stored at -20 °C.

For the expression of ERK2, the plasmid encoding tagged ERK2 in pQE80 was transformed into *E. coli* BL21(DE3) competent cells. Overnight cultures were sub-cultured into 1 L LB medium supplemented with 100 μg/mL ampicillin to a starting OD_{600} of 0.02, and cultures were grown at 37 °C with agitation at 250 RPM until they reached OD_{600} 1.0. Protein expression was induced with 1 mM IPTG and cultures were grown at 22 °C for 6 hours with agitation at 250 RPM. Bacterial cell pellets were harvested by centrifugation and stored at -20 °C.

For all protein purifications, cell pellets were resuspended in 40 mL 10 mM imidazole, 300 mM NaCl, 50 mM NaH_2PO_4, pH 8 and lysed by treatment with lysozyme and sonication on ice. Cell debris was removed by centrifugation and the supernatant was sterile filtered. All proteins were purified from clarified lysate using Ni-NTA agarose resin (Qiagen) following the manufacturer's recommendations. ERK2 was buffer exchanged into 50 mM HEPES, 100 mM NaCl, 20 mM $MgCl_2$, 10% glycerol, pH 7.4 using PD-10 desalting columns (Bio-Rad). MEK was further purified by gel filtration chromatography using a superdex 75 16/600 column (GE Healthcare Life Sciences) equilibrated with 50 mM HEPES, 100 mM NaCl, 20 mM $MgCl_2$, 10% glycerol, pH 7.4. Aliquots of 5-50 μL were snap frozen in liquid nitrogen and stored at -80 °C until use in phosphorylation reactions.

In vitro phosphorylation reactions

MEK-ERK phosphorylation reactions were carried out in 50 mM HEPES, 100 mM NaCl, 20 mM $MgCl_2$, and 1 mM ATP (pH 7.4). For MEK:ERK ratios of 1:5 and 1:10, 2 μM MEK was reacted with 10 μM ERK2 and 20 μM ERK2 respectively. Reactions were initiated by the addition of MEK into a master mix containing ERK and phosphorylation buffer, and ran for 90 minutes at 30°C. Reaction aliquots were diluted 4-fold in 8M Urea to terminate the reaction. Four separate reactions were run for the data presented in Supplementary Table 1.

Western blotting

4× SDS loading buffer was added to the reaction aliquots and immunoblotting was performed using standard techniques onto LF PVDF membrane. Primary anti-MEK antibody (1:4000; Cell Signaling Technology, 8727S), anti-dpERK antibody (1:4000; Cell

Signaling Technology, 4370S), and anti-ERK antibody (1:4000; Cell Signaling Technology, 4695S) were used to track the formation of total MEK, dpERK, and ERK respectively. Alexa Fluor conjugates (1:2000; Invitrogen) were used as secondary antibodies and membranes were imaged using a Biorad ChemiDoc MP Imaging System.

Fly stocks

Five mutations were introduced into a cDNA of Dsor1 (a gift from Dr. Veraksa (UMB, Boston)) with site-directed mutagenesis using the Phusion enzyme (NEB) and verified by sequencing. Wild type and mutant versions were cloned into the transformation vector pTIGER[29] between the NheI and XbaI restriction sites. These constructs were integrated into the 2nd chromosome using the φC31-based integration system[30], at the Attp site estimated to be at 25C6. UAS-MEK^{RNAi} (Bloomington stock # 36099), Histone-GFP, Tor^{D4021}/+ (a gift from Dr. Jimenez (IBMB, Barcelona)), UAS-PTTH (a gift from Dr. Warr (Monash University, Victoria)) were also used in the experiments. MTD-Gal4 (Bloomington stock # 31777), P(matα-GAL-VP16)mat67; P(matα-GAL-VP16)mat15[31] and nos-Gal4 (Bloomington stock # 32563) were used to drive expression in the early embryo.

Zebrafish injections

In pCS2(+) (Invitrogen), the EcoRI site was switched to EcoRV, and human MEK1 (a gift from Dr. Seger (Weizmann Institute, Rehovot)) was subsequently cloned between the BamHI and EcoRV restriction sites, while mCherry was cloned between the EcoRV and XhoI restriction sites. The set of 3 mutations were introduced into this construct with site-directed mutagenesis using the Phusion enzyme (NEB). The plasmids were then linearized using Not1, and synthetic capped mRNA was synthesized using the SP6 RNA polymerase mMessage mMachine kit (Ambion) and purified using the TRIzol reagent. Microinjection of 500 pL of the RNA mixture at a concentration of ~110 pg/nL (i.e. 55 pg) was performed using the PV280 Pneumatic PicoPump (World precision instruments). Embryos were acquired by pair mating of PWT fish. Established zebrafish protocols were adhered to in accordance with the Princeton University Institutional Animal Care and Use Committee.

Cuticle preparation

Embryos were dechorionated after being aged for more than 24 hours. Dechorionated embryos were shaken in methanol and heptane (1:1) and incubated overnight in a media containing lactic acid and Hoyer's media (1:1) at 65°C. Embryos were imaged on a Nikon Eclipse Ni.

Immunostaining and fluorescent *in situ* hybridization (FISH)

Drosophila—Antibody staining and FISH protocols were performed as described elsewhere[32]. Rabbit anti-dpERK (1:100; Cell Signaling Technology, 4370S), rabbit anti-ERK (1:100; Cell Signaling Technology, 4695S), rabbit anti-MEK (1:100; Cell Signaling Technology, 8727S), sheep anti-GFP (1:1000, Bio-Rad, 4745-1051), rabbit anti-GFP (1:1000, Life Technologies, A11122), sheep anti-digoxigenin (DIG) (1:125; Roche), and mouse anti-biotin (1:125; Jackson Immunoresearch) were used as primary antibodies. DAPI

(1:10,000; Vector laboratories) was used to stain for nuclei, and Alexa Fluor conjugates (1:500; Invitrogen) were used as secondary antibodies.

Zebrafish—Rabbit anti-dpERK (1:100; Cell Signaling Technology, 4370S), rabbit anti-ERK (1:100; 1:100; Cell Signaling Technology, 4695S), and rat anti-mCherry (1:1000; Life Technologies, M11217) were used as primary antibodies. The zebrafish immunofluorescence protocol is as follows: the embryos, staged at 50% epiboly, were washed twice in 1X PBST (1X PBS containing 0.1% Tween -20), transitioned to 100% MeOH, and stored at -20°C overnight. These embryos were transitioned into PBST by performing five minute washes in 75% MeOH:25% 1X PBST, 50% MeOH: 50% 1X PBST, 25% MeOH:75% 1X PBST, and 1X PBST. The embryos were washed three more times in 1X PBST at five minutes per wash. The embryos were blocked for 2 hours in 1X PBDT (1X PBST containing 1% DMSO) containing 10% normal sheep serum (NSS). The embryos were then incubated overnight in 1X PBDT containing the appropriate dilution of the primary antibody at 4°C. The embryos were quickly washed in 1X PBDT containing 1% NSS and 0.1M NaCl followed by five more 30 minute washes. The embryos were then washed for 30 minutes in 1X PBDT containing 1% NSS (1X PBDT-NSS), followed by an overnight incubation in 1X PBDT-NSS containing a 1:400 dilution of the appropriate Alexa Fluor secondary antibody at 4°C. The embryos were then washed in 1X PBDT containing 1% NSS and 0.1M NaCl for one minute followed by five more 30 minute washes. The final wash was in 1X PBDT for 30 minutes. For epiboly stage embryos, all steps were performed in glass specimen vials, as opposed to microfuge tubes, as this was found to better preserve embryo structure. In addition, the transitioning to and from methanol was not done for epiboly stage embryos.

Microscopy and image processing

Drosophila—Fluorescent imaging was performed on a Nikon A1-RS scanning confocal microscope with a 20× objective. For pairwise comparisons of wild type and mutant backgrounds, embryos were collected, stained, and imaged together under the same experimental conditions. Broken embryos, embryos with intact vitelline membrane, or embryos undergoing mitosis were excluded from the analysis.

Heatmap reconstruction—Pre-cellularization embryos were timed based on the surface nuclear density as revealed by DAPI staining, using a previously described image processing toolbox[33]. Nuclear cycle 14 embryos were timed based on the membrane invagination progression during the cellularization, as described previously[32]. Membrane length in the fixed embryos was measured from phase-contrast images. Using a combination of these two independent time markers, we obtained ten pooled time-stamped fluorescent intensities for four different positions (x_i) from anterior (x = 0) to the middle (x = 0.5) of the embryo. Fluorescent Intensities (FI) were normalized using the following formula:

$$\text{Normalized FI} = \frac{\text{FI} - \text{FI}_{\min}}{\text{FI}_{\max} - \text{FI}_{\min}}$$

Here FL_{min} and FL_{max} correspond to global minimum and maximum intensity respectively from WT and the respective mutant background. Normalized space-time fluorescent intensities were entered in MATLAB (R2015b, The Mathworks, Natick, Massachusetts). Matrix smoothing was performed using the MATLAB command *fit* with *loess* smoothing method and a span of 1 to generate heatmaps in Figure 5. To obtain heatmaps for ratio plots, smoothened heatmaps for WT and mutant were divided against each other. For more details, see the Supplementary Fig. 12.

Spatial profiles—Nuclear cycle 14 embryos were staged using membrane length as the independent time marker such that all embryos were within ~15 minutes of each other.

Cuticle imaging was performed with Nikon Eclipse Ni. Calculation of the posterior *tailless* domain was performed using a previously described protocol[34].

Zebrafish—Fluorescent imaging was performed on a Nikon A1-RS scanning confocal microscope with a 10× objective. For pairwise comparisons of uninjected and injected embryos, they were fixed, stained, and imaged together under the same experimental conditions. Broken embryos were excluded from the analysis.

Mathematical model

The primary purpose of formulating the model was to qualitatively capture the observed divergent effects of constitutively active mutations on developmental signaling. The model includes two types of inputs: u(x,t), which is a ligand-dependent pulse and is regulated in space and time, and is the same for WT and mutants, and u_0, which is invariant in space and time and represents the constitutive activity of the pathway. We relied on the experimentally reconstructed heatmap of ERK activation in WT to infer the timescale and length scale for u(x,t) (Supplementary Table 3). Importantly, no parameter fitting was performed. These two inputs result in a signal (S) which decays with a rate constant (k) and generates a negative feedback (I) with a feedback strength (a). The negative feedback could be either transcriptional[35,36] and/or post-translational[37–44], but our model does not discriminate between different types of pathway inhibition. Signaling dynamics in space and time is governed by two coupled differential equations:

$$\frac{dS}{dt} = \frac{u_o + u(x,t)}{1+I} - kS$$
$$\frac{dI}{dt} = aS$$

Differential equations were solved with the zero initial conditions for both variables (S and I). Details on the model parameters and functions is presented in Supplementary Table 3 and Supplementary Fig. 11.

Cilia measurements

Zebrafish embryos were fixed overnight at 14 hours post fertilization (10-somite stage) in 4% PFA at 4°C and the immunofluorescence protocol, as described earlier, was performed with mouse anti-acetylated-α-tubulin. The embryos were flat-mounted according to a

previously published protocol[45]. The yolk was first removed from the embryos and then they were flattened in Aqua Poly/Mount (Polysciences 18606) using a microscope slide, making sure that the ventral side was toward the coverslip. The embryos were imaged through the ventral side on a Nikon A1-R scanning confocal microscope. The Measurement Points feature of Imaris was used to accurately measure cilia length, even if the cilia pointed in the z-direction, by marking points along the cilia.

Code availability

The differential equations corresponding to the mathematical model were solved numerically, using the *ode15s* subroutine in MATLAB.

Data availability

Fly and zebrafish strains, and reagents are available upon request.

Supplementary Material

Refer to Web version on PubMed Central for supplementary material.

Acknowledgments

We thank Cori Hasty, Phillip Johnson, John London, and LAR staff for zebrafish care; Alexey Veraksa, Rony Seger, and Elizabeth Goldsmith for wild type MEK and ERK constructs; Maira Cardoso for help with the fluorescent *in situ* hybridization (FISH) probes; and Dr. Gary Laevsky and the Molecular Biology Confocal Microscopy Facility, which is a Nikon Center of Excellence, for microscopy support. We thank Elizabeth Goldsmith, Alexey Veraksa, Bruce Gelb, Rony Seger, John Humphreys, and Henry Mattingly for helpful discussions. S.Y.S. and A.S.F. thank Jamie Link for his input during the initial stages of this project. Y.G., K.Y., E.Y., A.S.F, and S.Y.S. were supported by the National Institutes of Health Grant R01 GM086537. G.A.J. acknowledges support from an NSF Graduate Research Fellowship under Grant No. DGE 1148900. R.D.B. was supported by the National Institutes of Health Grants R01 HD048584 and R01GM086537. J.L.P. was supported by the National Institutes of Health Grant R01 HD048584. T.S. was supported by the National Institutes of Health Grant R01 GM077620.

References

1. Rauen KA. The RASopathies. Annu Rev Genomics Hum Genet. 2013; 14:355–69. [PubMed: 23875798]
2. Tartaglia M, et al. Mutations in PTPN11, encoding the protein tyrosine phosphatase SHP-2, cause Noonan syndrome. Nat Genet. 2001; 29:465–468. [PubMed: 11704759]
3. Chen X, et al. Endogenous expression of Hras(G12V) induces developmental defects and neoplasms with copy number imbalances of the oncogene. Proc Natl Acad Sci U S A. 2009; 106:7979–84. [PubMed: 19416908]
4. Jindal GA, Goyal Y, Burdine RD, Rauen KA, Shvartsman SY. RASopathies : unraveling mechanisms with animal models. Dis Model Mech. 2015; 8:769–782. [PubMed: 26203125]
5. Rodriguez-Viciana P, et al. Germline mutations in genes within the MAPK pathway cause cardio-facio-cutaneous syndrome. Science. 2006; 311:1287–90. [PubMed: 16439621]
6. Nikolaev SI, et al. Exome sequencing identifies recurrent somatic MAP2K1 and MAP2K2 mutations in melanoma. Nat Genet. 2011; 44:133–139. [PubMed: 22197931]
7. Seger R, et al. Purification and Characterization of Mitogen-activated Protein Kinase Activator(s) from Epidermal Growth Factor-stimulated A431 Cells. J Biol Chem. 1992; 267:14373–14381. [PubMed: 1321146]
8. Gabay L, Seger R, Shilo BZ. MAP kinase in situ activation atlas during Drosophila embryogenesis. Development. 1997; 124:3535–41. [PubMed: 9342046]

9. Casanova J, Struhl G. Localized surface activity of torso, a receptor tyrosine kinase, specifies terminal body pattern in Drosophila. Genes Dev. 1989; 3:2025–38. [PubMed: 2560750]
10. Furriols M, Casanova J. In and out of Torso RTK signalling. EMBO J. 2003; 22:1947–52. [PubMed: 12727862]
11. Strecker TR, Halsell SR, Fisher WW, Lipshitz HD. Reciprocal effects of hyper- and hypoactivity mutations in the Drosophila pattern gene torso. Science. 1989; 243:1062–6. [PubMed: 2922596]
12. de las Heras JM, Casanova J. Spatially distinct downregulation of Capicua repression and tailless activation by the Torso RTK pathway in the Drosophila embryo. Mech Dev. 2006; 123:481–486. [PubMed: 16753285]
13. Klingler M, Erdélyi M, Szabad J, Nüsslein-Volhard C. Function of torso in determining the terminal anlagen of the Drosophila embryo. Nature. 1988; 335:275–277. [PubMed: 3412488]
14. Schupbach T, Wieschaus E. Germline autonomy of maternal-effect mutations altering the embryonic body pattern of Drosophila. Dev Biol. 1986; 113:443–448. [PubMed: 3081391]
15. Degelmann A, Hardy PA, Perrimon N, Mahowald AP. Developmental analysis of the torso-like phenotype in Drosophila produced by a maternal-effect locus. Dev Biol. 1986; 115:479–489. [PubMed: 3709971]
16. de Las Heras JM, Martinho RG, Lehmann R, Casanova J. A functional antagonism between the pgc germline repressor and torso in the development of somatic cells. EMBO Rep. 2009; 10:1059–65. [PubMed: 19644502]
17. Perrimon N, Engstrom L, Mahowald AP. A pupal lethal mutation with a paternally influenced maternal effect on embryonic development in Drosophila melanogaster. Dev Biol. 1985; 110:480–491. [PubMed: 3926563]
18. Sturm OE, et al. The mammalian MAPK/ERK pathway exhibits properties of a negative feedback amplifier. Sci Signal. 2010; 3:ra90. [PubMed: 21177493]
19. Amit I, et al. A module of negative feedback regulators defines growth factor signaling. Nat Genet. 2007; 39:503–12. [PubMed: 17322878]
20. Rewitz KF, Yamanaka N, Gilbert LI, O'Connor MB. The insect neuropeptide PTTH activates receptor tyrosine kinase torso to initiate metamorphosis. Science. 2009; 326:1403–5. [PubMed: 19965758]
21. Snyder-Warwick AK, et al. Analysis of a gain-of-function FGFR2 Crouzon mutation provides evidence of loss of function activity in the etiology of cleft palate. Proc Natl Acad Sci. 2010; 107:2515–2520. [PubMed: 20133659]
22. Xing L, et al. Layer specific and general requirements for ERK/MAPK signaling in the developing neocortex. Elife. 2016; 5
23. Krens SFG, et al. Distinct functions for ERK1 and ERK2 in cell migration processes during zebrafish gastrulation. Dev Biol. 2008; 319:370–83. [PubMed: 18514184]
24. Neugebauer JM, Amack JD, Peterson AG, Bisgrove BW, Yost HJ. FGF signalling during embryo development regulates cilia length in diverse epithelia. Nature. 2009; 458:651–654. [PubMed: 19242413]
25. Bonetti M, et al. Noonan and LEOPARD syndrome Shp2 variants induce heart displacement defects in zebrafish. Development. 2014; 141:1961–70. [PubMed: 24718990]
26. Baynam G, et al. A germline MTOR mutation in Aboriginal Australian siblings with intellectual disability, dysmorphism, macrocephaly, and small thoraces. Am J Med Genet A. 2015; 167:1659–67. [PubMed: 25851998]
27. Gripp KW, et al. Truncating mutations in the last exon of NOTCH3 cause lateral meningocele syndrome. Am J Med Genet A. 2015; 167A:271–81. [PubMed: 25394726]
28. Calebiro D, et al. PKA catalytic subunit mutations in adrenocortical Cushing's adenoma impair association with the regulatory subunit. Nat Commun. 2014; 5:5680. [PubMed: 25477193]
29. Ferguson SB, Blundon MA, Klovstad MS, Schüpbach T. Modulation of gurken translation by insulin and TOR signaling in Drosophila. J Cell Sci. 2012; 125:1407–19. [PubMed: 22328499]
30. Bischof J, Maeda RK, Hediger M, Karch F, Basler K. An optimized transgenesis system for Drosophila using germ-line-specific phiC31 integrases. Proc Natl Acad Sci U S A. 2007; 104:3312–7. [PubMed: 17360644]

31. Hunter C, Wieschaus E. Regulated expression of nullo is required for the formation of distinct apical and basal adherens junctions in the Drosophila blastoderm. J Cell Biol. 2000; 150:391–401. [PubMed: 10908580]
32. Lim B, et al. Dynamics of Inductive ERK Signaling in the Drosophila Embryo. Current Biology. 2015; 25
33. Coppey M, Boettiger AN, Berezhkovskii AM, Shvartsman SY. Nuclear trapping shapes the terminal gradient in the Drosophila embryo. Curr Biol. 2008; 18:915–9. [PubMed: 18571412]
34. Kim Y, et al. Context-dependent transcriptional interpretation of mitogen activated protein kinase signaling in the Drosophila embryo. Chaos. 2013; 23:25105.
35. Camps M, et al. Catalytic Activation of the Phosphatase MKP-3 by ERK2 Mitogen-Activated Protein Kinase. Science. 1998; 280:1262–1265. (80-.). [PubMed: 9596579]
36. Hacohen N, Kramer S, Sutherland D, Hiromi Y, Krasnow M. A sprouty Encodes a Novel Antagonist of FGF Signaling that Patterns Apical Branching of the Drosophila Airways. Cell. 1998; 92:253–263. [PubMed: 9458049]
37. Northwood IC, Gonzalezs FA, Wartmann M, Radensll L, V RJD. Isolation and Characterization of Two Growth Factor-stimulated Protein Kinases That Phosphorylate the Epidermal Growth Factor Receptor at Threonine 669. J Biol Chem. 1991; 266:15266–15276. [PubMed: 1651322]
38. Zakrzewska M, et al. ERK-Mediated Phosphorylation of Fibroblast Growth Factor Receptor 1 on Ser 777 Inhibits Signaling. 2013; 6:1–16.
39. Mckay MM, Ritt DA, Morrison DK. Signaling dynamics of the KSR1 scaffold complex. Proc Natl Acad Sci U S A. 2009; 106:11022–11027. [PubMed: 19541618]
40. Lax I, et al. The Docking Protein FRS2a Controls a MAP Kinase-Mediated Negative Feedback Mechanism for Signaling by FGF Receptors. Mol Cell. 2002; 10:709–719. [PubMed: 12419216]
41. Langlois WJ, Sasaoka T, Saltiel AR, Olefsky JM. Negative Feedback Regulation and Desensitization of Insulin- and Epidermal Growth Factor- stimulated p21ras Activation. J Biol Chem. 1995; 270:25320–25323. [PubMed: 7592690]
42. Dougherty MK, et al. Regulation of Raf-1 by Direct Feedback Phosphorylation. Mol Cell. 2005; 17:215–224. [PubMed: 15664191]
43. Ritt DA, Monson DM, Specht SI, Morrison DK. Impact of Feedback Phosphorylation and Raf Heterodimerization on Normal and Mutant B-Raf Signaling. Mol Cell Biol. 2010; 30:806–819. [PubMed: 19933846]
44. Brunet A, Pages G, Pouyssegur J. Growth factor-stimulated MAP kinase induces rapid retrophosphorylation and inhibition of MAP kinase kinase (MEK1). FEBS Lett. 1994; 346:299–303. [PubMed: 8013650]
45. Jaffe, KM., Thiberge, SY., Bisher, ME., Burdine, RD. Methods in Cell Biology. Vol. 97. Elsevier Inc.; 2010. Imaging Cilia in Zebrafish.

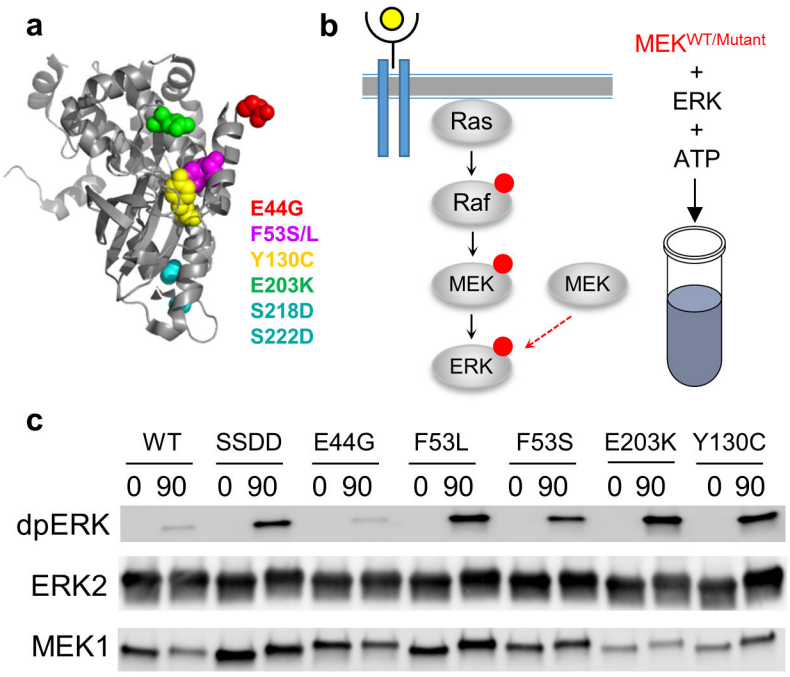

Figure 1.

MEK mutations are constitutively active *in vitro.* (**a**) The location of a set of mutations (E44G, F53S, F53L, Y130C, E203K, S218D/222D) (accession NM_002755.3) is shown in the structure of MEK1 (PDB file 3w8q). (**b**) (left) Schematic of the Ras pathway depicting MEK-mediated ERK activation by ligands (black, solid arrows) or by ligand-independent constitutively active MEK (red, dashed arrow). (right) Schematic of the *in vitro* system. (**c**) ERK2 activation by the wild type (WT) MEK1 and the MEK1 variants as detected by a western blot of samples of the reconstituted system with purified proteins. With the exception of E44G, MEK1 variants associated with diseases result in ligand-independent ERK activation, which was higher than WT MEK1. MEK1 S218D/S222D, a phosphomimetic variant, was used as a positive control. Four experimental replicates were performed for MEK:ERK ratio of 1:5. Blot images in (**c**) were cropped for bands corresponding to MEK1, ERK2, and dpERK. Additional quantifications of dpERK levels are presented in the Supplementary Tables 1 and 2.

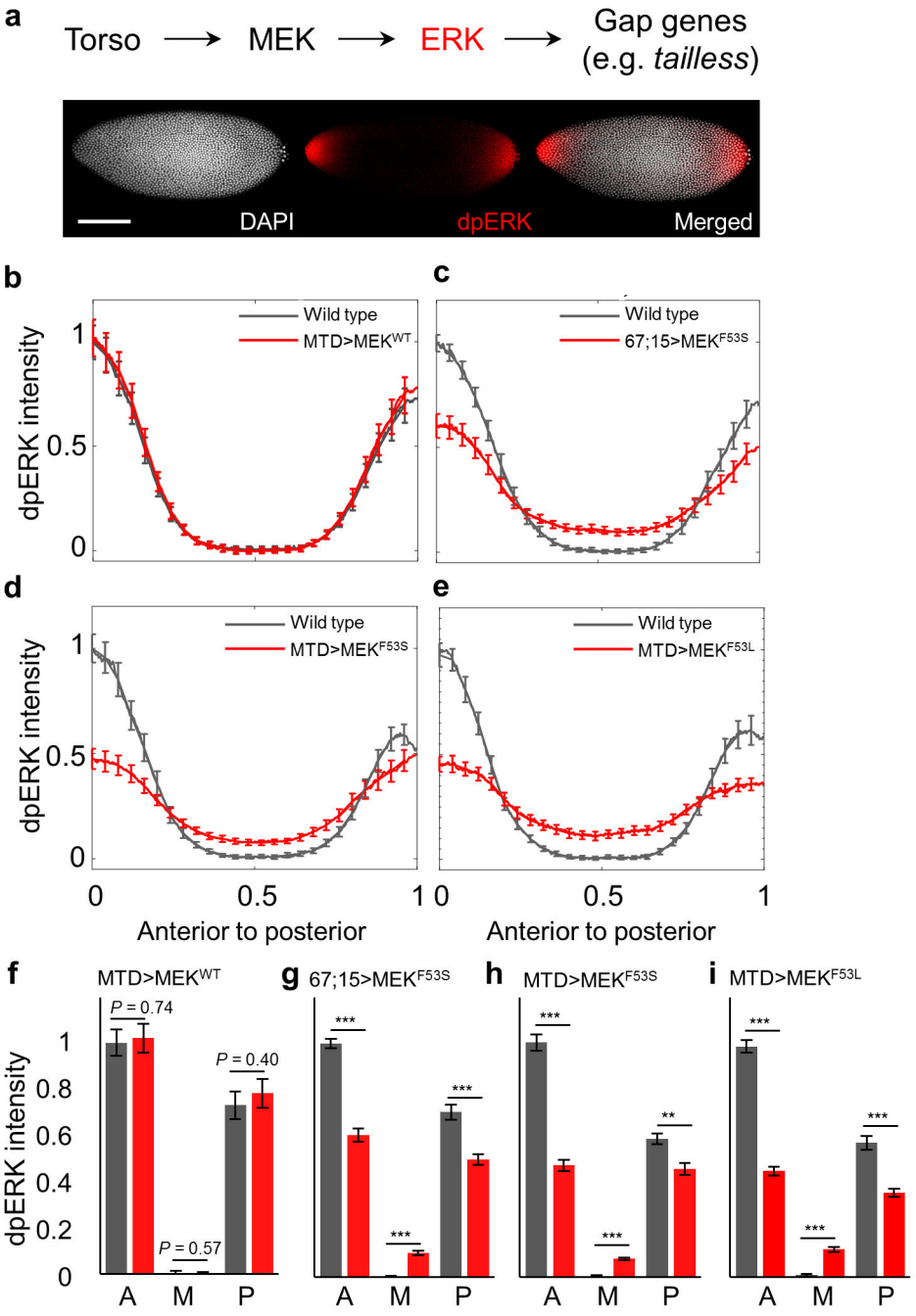

Figure 2.

MEK mutations cause divergent effects on ERK activation *in vivo*. (**a**) Torso RTK signaling in the *Drosophila* embryo. A nuclear cycle 14 WT embryo stained for DAPI and dpERK (See Supplementary Figs. 3,4 for details of embryo staging). Scale bar, 100 μm. (**b**) Overexpression of WT MEK does not alter the dpERK profile. (**c-e**) Overexpression of MEK mutations F53S (**c,d**) and F53L (**e**) result in opposing effects in the middle and pole regions of the embryo. Pairwise comparisons of the dpERK profiles for (**b**) WT (n = 15) and MTD>MEK^{WT} (n = 17); (**c**) WT (n = 10) and 67;15>MEK^{F53S} (n = 19); (**d**) WT (n = 8) and

MTD>MEK^{F53S} (n = 20); (**e**) WT (n = 19) and MTD>MEK^{F53L} (n = 24). Error bars denote standard error of the mean (s.e.m.). **(f-i)** Comparative analysis of the dpERK levels at the anterior (A), middle (M), and posterior (P) regions of the embryo. Overexpression of MEK variants using maternal drivers does not affect total ERK levels (Supplementary Fig. 5). *P* values, Student's t-test (two-sided, homoscedastic): ***$P < 0.00001$, **$P = 0.0036$. Error bars denote standard error of the mean (s.e.m.).

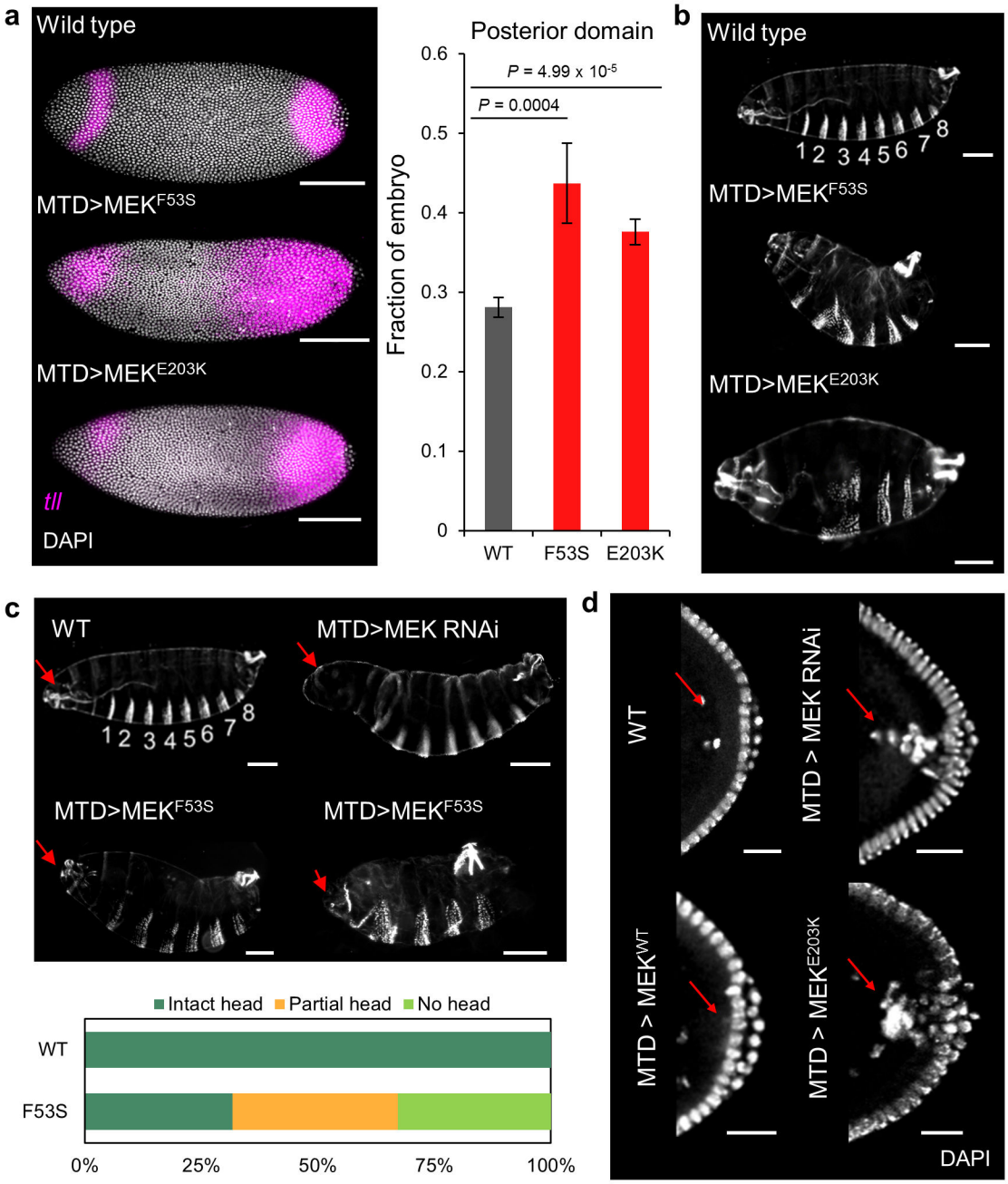

Figure 3.

Opposing effects of activating mutations on the ERK-dependent morphological phenotypes. (**a**) (left) Expression of *tailless* (magenta) is expanded, more prominently at the posterior, in MEK mutants (data shown for F53S and E203K). Scale bar, 100 μm. (right) Quantification of the posterior tailless domain yields significant differences (n_{WT} = 15, n_{F53S} = 3, n_{E203K} = 19). Expression patterns of some other gap genes are not affected (Supplementary Figs. 8,9). *P* values, Student's t-test (two-sided, homoscedastic). Error bars denote standard error of the mean (s.e.m.). (**b**) Larval cuticles for the WT and MEK mutants F53S and E203K are shown. F53S (less than eight segments: 51/52 of the dead embryos); E203K (less than eight

segments: 63/68 dead embryos). (**c**) (top) Constitutively active MEK mutation F53S results in loss of anterior head structures (red arrows), a partially penetrant phenotype also observed in embryos lacking maternal MEK. (bottom) Quantification of anterior head structures for WT (n = 35) and F53S MEK mutant (n = 79). Scale bar, 100 μm. (**d**) WT (top left) and overexpressed MEK (bottom left, 17 out of 18 embryos are normal) embryos do not display pole-hole phenotype (red arrows), whereas both loss of MEK (top right, 4 out of 8 embryos display pole-hole phenotype) and overexpression of activating MEK mutant E203K (bottom right, 27 out of 39 embryos display pole-hole phenotype) result in a pole-hole phenotype. Scale bar, 25 μm.

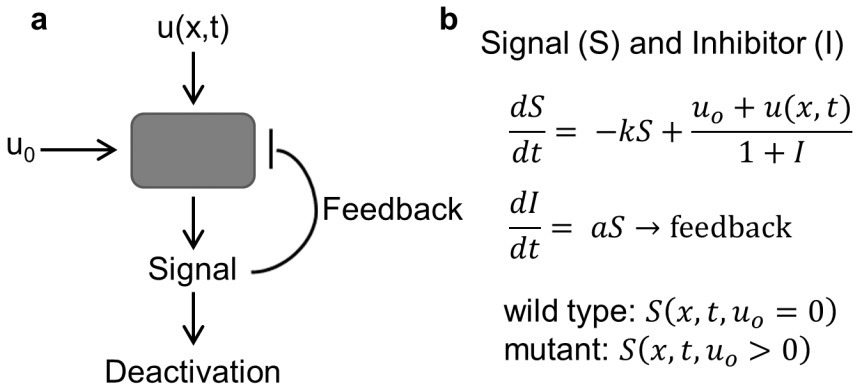

Figure 4.

A two-input mathematical model for feedback-induced effects on ERK signaling. (**a**) Schematic of the mathematical model of signal-induced feedback. (**b**) Differential equations governing the model; here u_0 and u(x,t) are ligand-independent and ligand-dependent inputs respectively. S: signal; I: Inhibitor; k: rate constant of signal degradation; a: strength of feedback. Additional modeling details and parameter values are provided in the Supplementary Table 3.

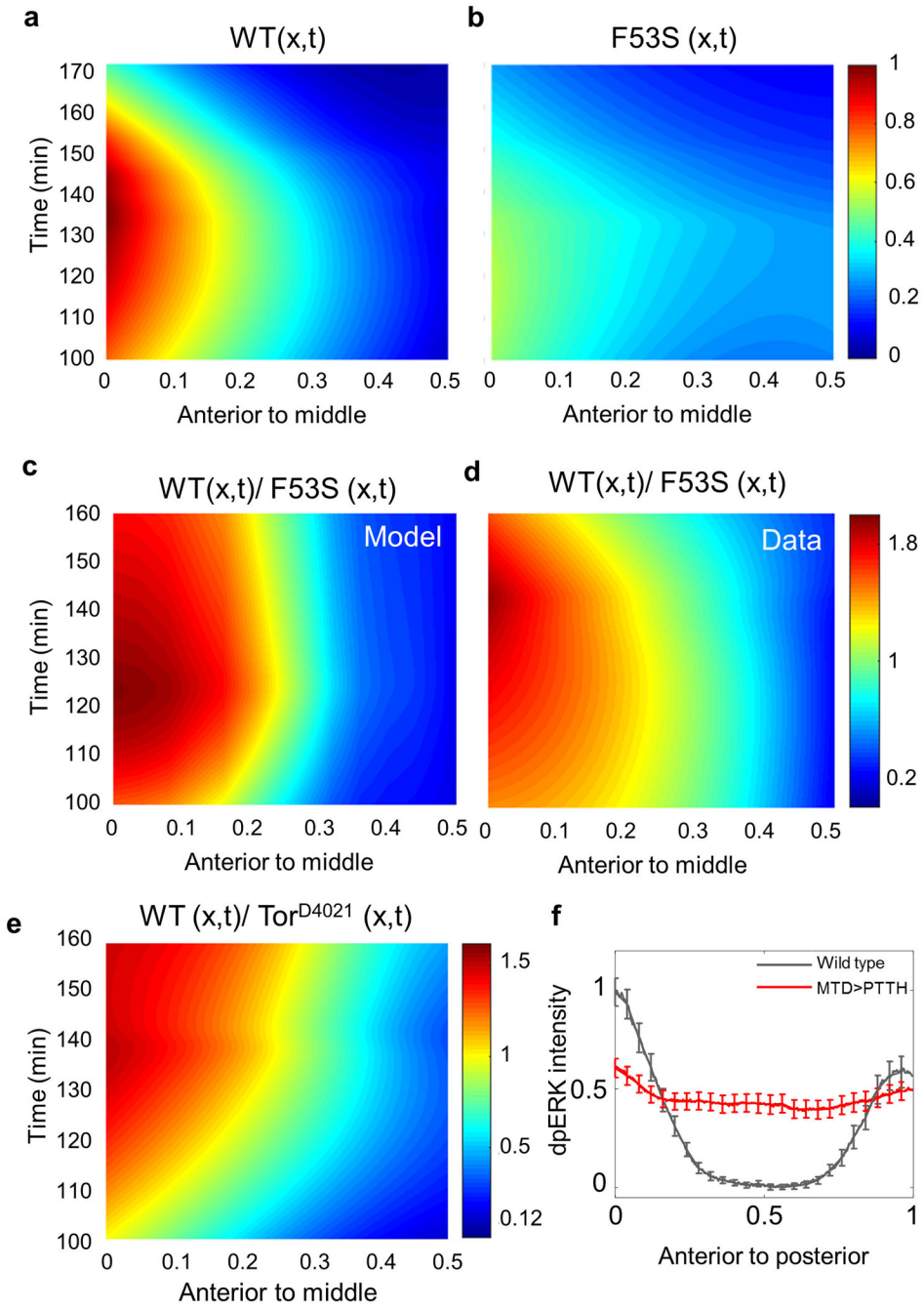

Figure 5.

A feedback-based mathematical model. (**a,b**) Heatmaps of the reconstruction of the spatiotemporal profile of ERK activation, from anterior (0) to the middle (0.5) in WT (n = 51) and MEK mutant F53S (n = 57) from snapshots of fixed *Drosophila* embryos (See Methods for details of reconstruction) (**c,d**) A heatmap of the ratio of dpERK intensity in WT embryos to that of embryos expressing MEK-F53S, generated by the model (**c**) and obtained from data (**d**). In both cases, the ratio changes from >1 (at the pole) to <1 (in the middle of the embryo). (**e**) A heatmap of the ratio of dpERK intensity in WT embryos to that

of embryos carrying a constitutively active mutation Tor^{D4021} ($n_{WT} = 55$, $n_{D4021} = 51$). Individual heatmaps for WT and Tor^{D4021} are shown in Supplementary Fig. 13. (**f**) Pairwise comparison of dpERK levels in the WT embryos (n = 16) and embryos expressing PTTH (n=28, see text for details). Error bars denote standard error of the mean (s.e.m.).

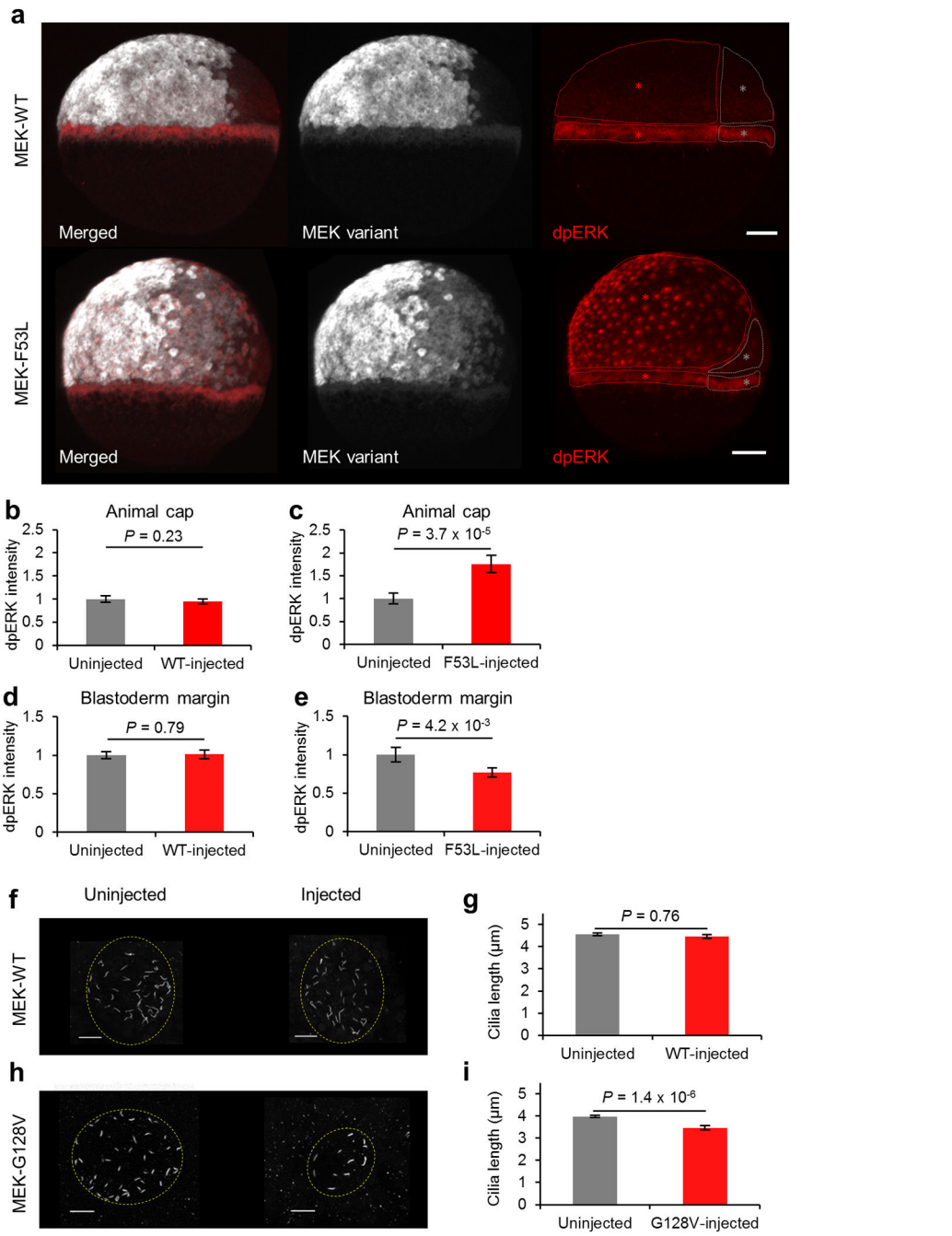

Figure 6.

MEK mutations cause divergent effects on ERK signaling in zebrafish. (**a**) Embryos injected with MEK constructs (gray) in one cell of the 2-cell stage embryo reveal divergent effects on ERK signaling (red) during epiboly. The domains affected by the injected constructs (red) are compared to signaling levels in areas that do not express the injected construct (gray) in (**b-e**). (**b,c**) In the animal cap, WT MEK1 does not affect dpERK levels (n = 13) (**b**), whereas the MEK1 variants F53L (n = 10) (**c**) and G128V (n = 8) (Supplementary Fig. 14a) result in increased dpERK levels. (**d,e**) In the blastoderm margin, WT MEK1 does not affect

dpERK levels (n = 15) (**d**), whereas the MEK1 variants F53L (n = 11) (**e**) and G128V (n = 8) (Supplementary Fig. 14) result in decreased dpERK levels. (**b-e**) *P* values, Student's t-test (two-sided, paired). Scale bar, 100 μm. (**f,g**) WT MEK1 does not affect cilia length in KV, which was measured at the 14-somite stage (16 hpf) (Uninjected: n = 6 embryos, 211 cilia; WT-injected: n = 4 embryos, 144 cilia). Scale bar, 10 μm. (**h,i**) However, the MEK1 G128V variant causes shorter cilia length in KV, which was measured at the 10-somite stage (14 hpf) (Uninjected: n = 6 embryos, 295 cilia; G128V-injected: n = 3 embryos, 67 cilia). In agreement with a previous study, we found a reduced number of cilia[25]. (**g,i**) *P* values, Student's t-test (two-sided, homoscedastic). Error bars denote standard error of the mean (s.e.m.).